2019

Grating Coupler for Surface Waves Based on Electrical Displacement Currents

Jonathan R. Brescia
University of Central Florida

GRATING COUPLER FOR SURFACE WAVES BASED ON ELECTRIC DISPLACEMENT CURRENTS

by

JONATHAN BRESCIA

A thesis submitted in partial fulfilment of the requirements
for the Honors in the Major Program in Physics
in the College of Sciences
and in the Burnett Honors College
at the University of Central Florida
Orlando, Florida

Fall Term, 2018

Thesis Chair: Dr. Robert Peale

ABSTRACT

Bound electromagnetic surface waves can be excited by free-space waves on a corrugated conduction surface. These electromagnetic surface waves, called surface plasmon polaritons (SPPs), are coupled to a plasma of free charges, which travel together with the wave. We investigated the effect of separating metal corrugations from the smooth metal ground plane with a thin dielectric layer, and we show that SPPs can be excited via displacement currents. However, the SPP excitation resonances broaden and disappear as the dielectric thickness approaches 1% of the wavelength.

TABLE OF CONTENTS

LIST OF FIGURES v

LIST OF TABLES vi

CHAPTER ONE: INTRODUCTION 1

Theoretical Considerations 1

CHAPTER TWO: LITERATURE REVIEW 4

CHAPTER THREE: METHODOLOGY 6

Device Fabrication 6

Device Infrared Characterization 9

FDTD Simulations 10

CHAPTER FOUR: RESULTS 11

CHAPTER FIVE: DISCUSSION 18

LIST OF REFERENCES 21

LIST OF FIGURES

Figure 1: SPP Dispersion Relation with Added Grating Momentum 3

Figure 2: Schematic of SPP Excitation in dielectric -Grating Structure [9] 5

Figure 3: Dielectric -Grating Device Schematic 6

Figure 4: IR Characterization Experimental Set-Up 9

Figure 5: Material Comparison of Dielectric Layer, Angular Sweep 11

Figure 6: Material Comparison of Dielectric Layer, Wavelength Sweep 11

Figure 7: Angular Sweep Dielectric Thickness Comparison, SiO_2 13

Figure 8: Angular Sweep Dielectric Thickness Comparison, TiO_2 13

Figure 9: Wavelength Sweep Dielectric Thickness Comparison, SiO_2 14

Figure 10: Wavelength Sweep Dielectric Thickness Comparison, TiO_2 14

Figure 11: Angular Sweep Dielectric Thickness Comparison, Sample Set 2 - Raw Reflectivity 15

Figure 12: Angular Sweep Dielectric Thickness Comparison, Sample Set 2 - Normalized 15

Figure 13: Simulation Data of Wavelength Sweep Dielectric Thickness Comparison, 12^o 17

Figure 14: Simulation Data of Wavelength Sweep Dielectric Thickness Comparison, 36^o&38^o 17

Figure 15: Published Optical Constants for SiO_2 and TiO_2 18

Figure 16: Measured Optical Constants for Dielectric Films Used in Sample Set 1 18

LIST OF TABLES

Table 1: List of Devices with Pertinent Parameters 8

Table 2: List of Equipment Used..... 9

Table 3: Published Optical Constants for SiO_2 and TiO_2 at Important Wavelengths 19

CHAPTER ONE: INTRODUCTION

A transverse magnetic (TM, H wave, p-polarized) electromagnetic wave can be propagated along a plane boundary between two media whose permittivities have opposite sign, e.g. at the interface between a lossless dielectric $\varepsilon_d > 0$ and metal $\mathrm{Re}[\varepsilon_m] < 0$. The wave is exponentially damped without dissipation away from the interface into both media. The wave is bound to free charges in the metal surface, and these charges propagate with the wave [1, 2], leading to dissipation and exponential damping in the direction of propagation. The coupling of surface wave to surface plasma leads to a characteristic polariton dispersion relation, and the waves are called surface plasmon polaritons (SPP). Because the SPP electromagnetic fields must drag the plasma along with them as they propagate, SPPs travel more slowly than free space waves of the same frequency. Due to this momentum mismatch, SPPs cannot be excited on smooth surfaces by free-space beams of the same frequency. However, corrugations on the metal surface can add or subtract momentum from those beams, allowing them to conserve momentum and excite SPPs. When the corrugation is in the form of a regular pattern of period p, such as a grating, the momentum provided is in integral multiples of the grating wave vector $2\pi/p$.

Theoretical Considerations

SPP wavefunctions and dispersion relation are derived in [3]. Starting with Maxwell's equations in Gaussian units for monochromatic fields,

$$\boldsymbol{\nabla} \times \boldsymbol{E} = \frac{i\omega}{c} \boldsymbol{H} \tag{1}$$

$$\boldsymbol{\nabla} \times \boldsymbol{H} = \frac{-i\varepsilon\omega}{c}\,\boldsymbol{E} \tag{2}$$

we eliminate **E** by substituting (2) into (1), obtaining

$$\Delta\boldsymbol{H} + \frac{\varepsilon\omega^2}{c^2}\boldsymbol{H} + \left(\frac{1}{\varepsilon}\right)(\boldsymbol{\nabla}\varepsilon) \times (\boldsymbol{\nabla} \times \boldsymbol{H}) = 0 \tag{3}$$

We consider the one-dimensional case where ε varies in the direction perpendicular to a plane boundary, ε = ε(z), where the wave propagates in the xz plane, and where translational invariance along x yields dependence $e^{i\kappa x}$ with κ a constant. If **H** is perpendicular to the plane of propagation (y-direction), which is called TM polarization, H-waves, or p-polarization by different authors, equation (3) becomes

$$\frac{\partial}{\partial z}\left(\frac{1}{\varepsilon}\frac{\partial H}{\partial z}\right) + \left(\frac{\omega^2}{c^2} - \frac{\kappa^2}{\varepsilon}\right)H = 0 \tag{6}$$

Considering **H** wave along the interface of two materials that have permittivities of opposite signs (say a metal – dielectric boundary), $\varepsilon_1 > 0$ and $\varepsilon_2 < 0$, where the half space $z > 0$ contains the medium with the positive permittivity (ε_1), yields solutions

$$H_1 = H_0 e^{ikx - \kappa_1 z}, \quad \kappa_1 = \sqrt{k^2 - \frac{\omega^2\varepsilon_1}{c^2}} \quad for\ z > 0 \tag{7}$$

$$H_2 = H_0 e^{ikx - \kappa_2 z}, \quad \kappa_2 = \sqrt{k^2 + \frac{\omega^2|\varepsilon_2|}{c^2}} \quad for\ z < 0 \tag{8}$$

where k, κ_1, and κ_2 are real. The dispersion relation between k and ω is

$$k^2 = \frac{\omega^2\varepsilon_1|\varepsilon_2|}{c^2(|\varepsilon_2| - \varepsilon_1)} \tag{9}$$

This problem has no solution for **E**-waves, which do not propagate. The quanta of the **H**-waves are the SPPs.

Figure 1 presents a schematic of the SPP dispersion relation, line 1. Frequency is plotted vs the SPP wavevector k. It falls below the grazing-incidence light line, $\omega = ck$, line 2, which has slope c. Line 3 represents the dispersion relation for a light beam between normal and grazing incidence with slope $c/\sin\theta_i$, where θ_i is the incidence angle. Line 4 represents line 3 with one unit of grating momentum added. Only Line 4 has an intersection with line 1. This shows how a monochromatic beam of frequency ω incident on a metal grating at angle θ_i can couple to and excite an SPP at that frequency.

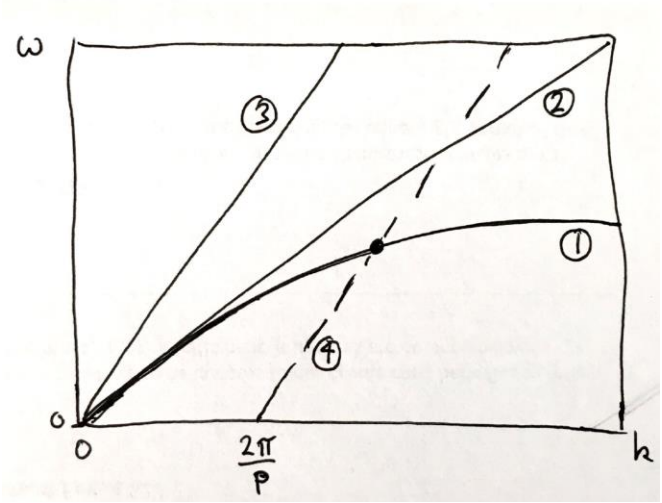

Figure 1: SPP Dispersion Relation with Added Grating Momentum

The equation relating the experimental parameters of SPP-grating coupling is provided below. [4] In this equation, θ is the incidence angle, λ the incidence wavelength, d the grating period, n the grating order (can be either positive or negative), and k_{spp} is the complex SPP wavevector as described in the previous paragraph.

$$Sin(\theta) + \frac{n\lambda}{d} = \pm\frac{c}{\omega} Re\left[k_{spp}\right] \tag{10}$$

CHAPTER TWO: LITERATURE REVIEW

A simple grating coupler for SPPs comprises metal stripes deposited on a smooth metal substrate. Optimum coupling occurs when the stripe heights are about 10% of the wavelength [4]. Then monochromatic beams incident on the surface at specific angles of incidence result in angularly narrow and deep absorption features. At the resonance angle, these can absorb all of the incident beam.

It was previously reported [4] that when metal grating stripes are deposited on an insulating substrate, so that neighboring metal stripes are completely electrically insulated, no SPP absorption resonances were observed. This was easily understood in that the insulating barriers prevented free charges from flowing together with the SPP electromagnetic wave. Nevertheless, other authors [5, 6, 7, 8, 9] have identified as SPPs certain absorption resonances on devices comprising metal grating strips insulated from an underlying smooth metal ground plane by a thin dielectric layer. A purpose of this thesis is to investigate whether such excitation is really possible, and under what conditions, by preparing and studying such devices with different thicknesses of dielectric layer. We find that it is possible to excite SPPs on such devices, but the excitation resonances quickly broaden and disappear as the thickness of the insulating layer approaches 1% of the wavelength.

We chose to operate at long-wave infrared frequencies where gratings of the required period can be fabricated by ordinary contact photolithography. The design of such grating couplers was studied and optimized by Cleary [4], who found that the grating height that maximizes the depth of the SPP absorption resonance monitored in reflectance while retaining narrow angular line width is ~10% of the wavelength.

Lamellar gratings comprising grating bars with rectangular cross section have spatial Fourier components in multiples of the grating fundamental, so that the incident beam can absorb multiples of grating momenta. The beam can also lose multiples of this momenta to the grating, and SPPs can travel in both directions perpendicular to the grating bars. In other words, a grating gives rise to multiple SPP excitation resonances.

This paper investigates whether it is necessary, for excitation of SPPs, for the metal grating bars to be electrically in contact with the smooth metal substrate. Since SPPs must drag along the charges that are coupled to the fields, SPPs do need a continuous conducting surface to propagate. However, the excitation of SPPs on a smooth continuous conductor may not require electrical continuity with the coupling structures. Displacement currents between the structures and a continuous underlying ground plane, as shown in Figure 2, may be able to excite SPPs. The incident beam would excite oscillating dipoles in the free-standing grating bars, and the fields of these dipoles would then excite the SPPs in the ground plane.

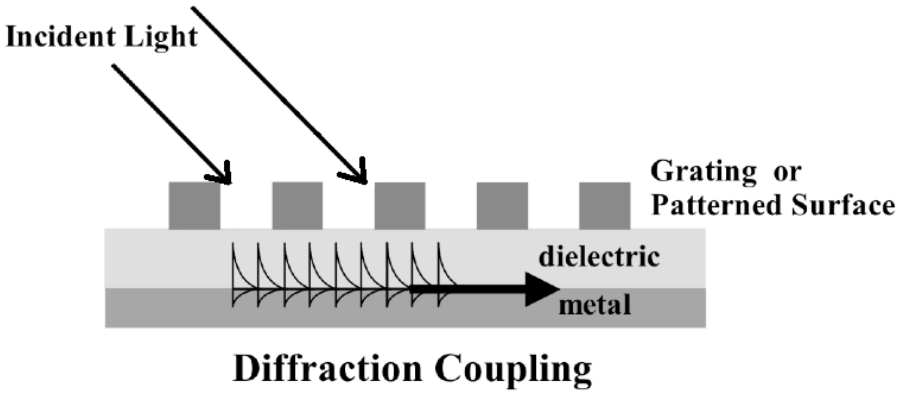

Figure 2: Schematic of SPP Excitation in dielectric -Grating Structure [9]

CHAPTER THREE: METHODOLOGY

Device Fabrication

Two sets of samples were fabricated using different facilities. The devices in sample set 1 were fabricated at the Air Force Research Laboratory (AFRL-RYDH) in Dayton, Ohio. The devices in sample set 2 were fabricated at Microdevice Prototyping Facility in the Physics Department of the University of Central Florida. Figure 3 presents a schematic device cross section. The dielectric thickness *t* is the parameter which was varied.

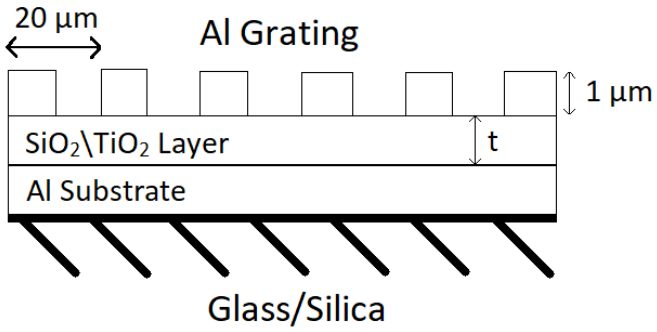

Figure 3: dielectric -Grating Device Schematic

In sample set 1 silicon wafers were used as substrates, and in sample set 2 glass microscope slides were used as substrates. These were chemically cleaned with acetone, methanol, and isopropanol in that order. Then they were dried using compressed nitrogen gas.

Next, the conducting ground plane was deposited. Optically thick aluminum was deposited on each sample to a height of no less than 200 nm. Al for sample set 1 was deposited by sputtering and Al for sample set 2 was deposited by electron-beam evaporation.

Next the samples had a layer of either SiO_2 or TiO_2 deposited on them by reactive sputtering in sample set 1, and by e-beam evaporation for sample set 2 to serve as dielectric spacer. The former has strong absorption at 9 microns wavelength, while the latter does not. Comparison will allow us to isolate the effect of dielectric absorption, if any. There were 6

samples built in sample set 1 with dielectric thicknesses of 20, 40, and 80 nm using both SiO_2 and TiO_2 as the material in the dielectric layer. There were 6 samples built in sample set 2 that have dielectric thicknesses that range from 40 to 640 nm in 6 steps, approximately doubling in thickness in each step. SiO_2 was the only dielectric material that was used in the construction of the samples in sample set 2. In addition to these 12 samples, a reference grating sample was built during the construction of sample set 2 without dielectric spacer.

The next step for all samples was deposition and patterning of aluminum lamellar grating bars. Positive-tone photoresist (S-1813) was spun onto substrates at 2000 rpm for 60 secs using an automatic, programmable spinner. These parameters were taken from the manufacturer specifications to obtain the >1 μm thickness desired for the lift-off step. The samples were then baked on a hot plate at 115°C for 120 seconds. Then samples were exposed to high intensity UV light through a mask to put the desired grating-bar image on the photoresist. The grating mask used has a period of 20 μm, which has been shown ideal for exciting SPPs using 10 μm IR radiation [4]. The amount of incident UV energy required to appropriately expose the photoresist (according to the manufacturer) is 120 mJ. The incident power from the UV light source can be directly measured, and an exposure time can be calculated from those two numbers. The 120 mJ of energy was an appropriate number for the control sample. Because the photoresist and the dielectric layer in sets 1 and 2 samples are UV transparent, there was a back reflection off the metal ground plane, resulting in more energy being delivered to the photoresist than if there was no reflection. Multiple trials were performed to optimize the exposure for each dielectric thickness.

After exposure, the samples were baked again at 115°C for 120 seconds. This promotes adhesion of the photoresist. UV-exposed regions are washed away during development in the

photoresist developer MF-CD-26. Typical development times are in the range of 30 to 45 seconds. This stage revealed if the exposure time was correct. If not, the photoresist was washed off using the cleaning procedure described above, and the photolithography process repeated.

After successful development, the sample was "de-scumed" in an oxygen plasma (Samco Reactive Ion Etcher). This ensures that the developed areas are clean so that the subsequently-evaporated metal will stick there, and it removes the rough edges of the photoresist. The process takes 12 seconds, with an O_2 flow rate of 5 sccm's.

Finally, 1 μm of Al was deposited by sputtering in sample set 1 and by e-beam evaporation in sample set 2 on the devices followed by lift-off in acetone in a sonicator. This process takes 5 to 20 minutes. Then the sample was cleaned to remove all the excess aluminum particles. A list of the devices made can be found in table 1.

Table 1. List of Devices with Pertinent Parameters

Device Inventory			
Device Number	Sample Set	Dielectric Material	Dielectric Thickness (nm)
EMS-SiO2-1	1	SiO_2	20
EMS-SiO2-2	1	SiO_2	40
EMS-SiO2-3	1	SiO_2	80
EMS062518-3	1	TiO_2	20
EMS062518-4	1	TiO_2	40
EMS062518-5	1	TiO_2	80
AF17Oct13	2	N/a	0
AF18May16(b)	2	SiO_2	40
AF18May17(a)	2	SiO_2	80
AF17Oct24	2	SiO_2	150
AF18May17(b)	2	SiO_2	320
AF18May22	2	SiO_2	640

Device Infrared Characterization

Figure 3 presents a schematic of the experimental set up. A list of the equipment used can be found in table 2. To characterize the excitation of infrared SPPs, we measured specular

reflection of a p-polarized (electric field in the plane of incidence) LWIR laser beam (spanning 7.52 to 9.70 µm wavelength). The invisible IR beam was coaligned with the visible beam of a laser diode to aid alignment. The position of the IR beam was found using thermally sensitive liquid crystal paper. The coalignment used a retractable mirror that was put in the beam path to reflect the visible light and then removed after alignment to allow the IR beam to reach the device. Then, several fixed mirrors were positioned to direct the shared beam path towards the device.

Table 2. List of Equipment Used

Equipment List	
1	Daylight Solutions QCL (7.52 - 8.52 µm)
2	Daylight Solutions QCL (9.50 - 10.2 µm)
3	Huber Motor Controled Double Goniometer
4	Discrete Pyros Detector (Room Temperature)
5	UHF Zurich Instruments Lock-in Amplifier

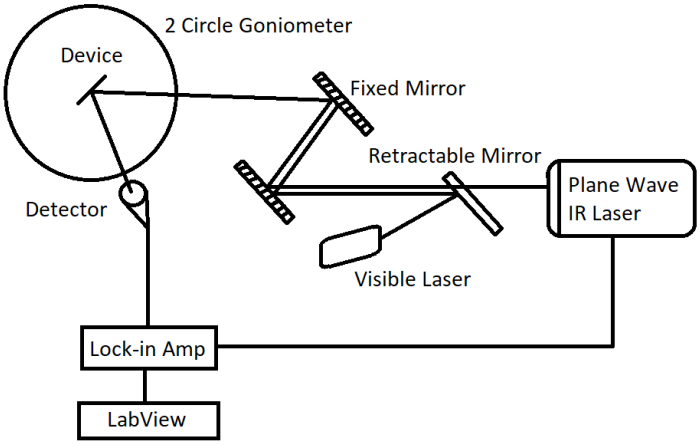

Figure 4: IR Characterization Experimental Set-Up

The devices were mounted on a Huber D-83253 motor controlled double goniometer for measurement of specular reflection as a function of incidence angle. The devices were aligned so that the principle beam (zeroth diffraction order) was back reflected to the source when $\theta = 0$.

The sample surface was positioned precisely at the goniometer center using a micrometer translation stage, so that as θ changed, the specularly-reflected spot was stationary on the detector mounted on the 2π arm.

The detector used was a room temperature Discrete Pyros Detector. Typical output voltages were in the range of 1 – 10 mV, well within the range of this detector so no signal attenuation was required. A gold mirror was used as a reflectance reference device. The 0^{th} order diffraction reflectance was calculated by dividing the voltage output measured by the detector by the reference to give values spanning 0 (complete absorption) to 1 (perfect reflection). The angle of each device was adjusted in order for the beam to be incident on the most sensitive part of the detector. Both angular and wavelength sweeps were performed and characterized.

The detector signal was monitored by a UHF Zurich Instruments Lock-in Amplifier, where the laser pulse frequency was used as the reference. This signal was collected in a LabView program. After the reference was divided out of the raw data, reflectivity was plotted verses incidence angle (with fixed incident wavelength) in the first case and verse wavelength (with fixed incidence angle) in the other to reveal absorption resonances.

FDTD Simulations

Finite-Difference Time-Domain (FDTD) simulations were performed to match the wavelength sweep experiments that were performed with sample set 1. Both the SiO_2 and the TiO_2 samples were simulated at an incidence angle of 12°, and the SiO_2 samples were further simulated at 36° and 38°.

CHAPTER FOUR: RESULTS

The infrared characterization data for sample sets 1 and 2 are plotted in figures 4-11. These figures show reflectivity as a function of angle with a fixed wavelength (Figs. 4, 6, 7, 10, and 11), and reflectivity as a function of wavelength at fixed angles (Figs. 5, 8, and 9). Figures 4-9 contain the characterization of sample set 1 and figures 10 and 11 shows the characterization of sample set 2. FDTD simulations were also performed with those results displayed in Figures 12 and 13. The simulations show reflectivity as a function of wavelength at fixed angles.

These experiments that are trying to characterize the plasmonic features of these dielectric-grating devices along two parameters, dielectric thickness and material. Figures 4 and 5 show a comparison between SiO_2 and TiO_2 as the materials in the dielectric layer, with the reference grating (no dielectric) shown for comparison. For all wavelengths and angles of incidence, the samples with the dielectric layer show a lower baseline reflectivity than the reference.

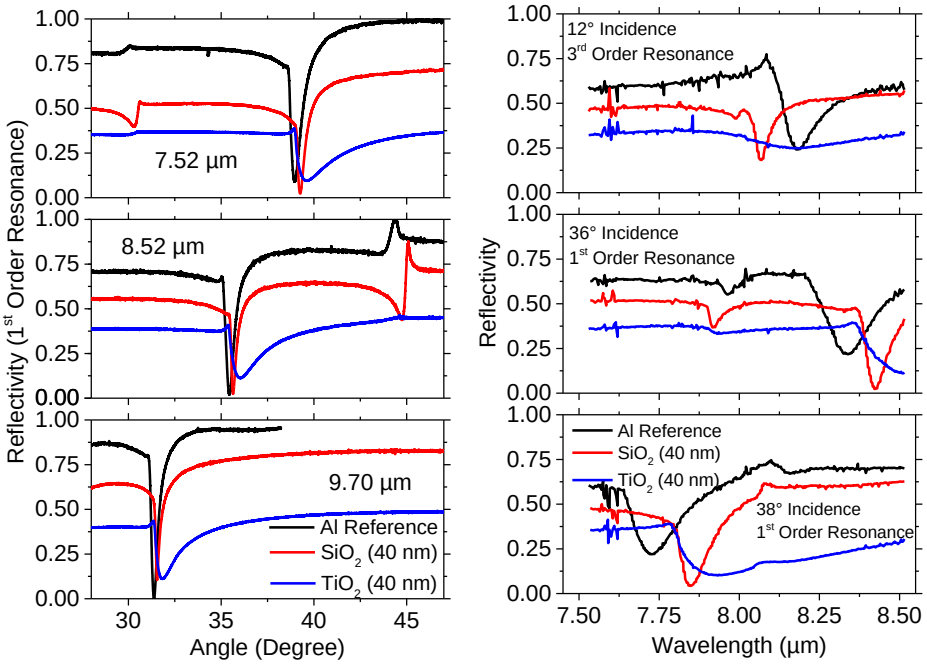

Figure 5(left), 6(right): Material Comparison of Dielectric Layer, Angular Sweep (Fig. 5) and Wavelength Sweep (Fig. 6)

The primary resonance angle for the angular sweep experiment is shown to be slightly shifted towards larger angles for the dielectric grating structures with TiO_2 showing a larger shift than SiO_2. The shift of the resonance for the TiO_2 in approximately 2^o for all three wavelengths. The resonance shift is also apparent in the wavelength sweep case where the peak of the resonance was shifted approximately 0.2 µm in the TiO_2 case (the more pronounced shift of the two dielectric materials). The direction of the shift is not uniform for the wavelength sweep case, as it was for the angular sweep characterization. The resonance observed at an incidence angle of 12^o shifts towards the shorter wavelengths, while the resonance at 36^o and 38^o both seem to shift towards longer wavelengths.

Figures 6-9 show a comparison of the effects on reflectivity as a function of dielectric thickness, with a side-by-side comparison of the two materials used. In every case, the baseline reflectivity of the devices decreases with increasing dielectric thickness. In both the angular and wavelength sweep trials, the resonance peak of the SiO_2 devices (Fig. 6 and Fig. 8) appears to

maintain its reflectivity level at the resonance position, with a slight shift in position for the wavelength sweep trial. The TiO_2 devices, shown next to the SiO_2 ones (Fig. 7 and Fig. 9), show an increase of reflectivity at the resonance position as dielectric thickness increases for both the angular and wavelength sweep trials. The resonance position of these samples seems to be constant, with a slight drift towards larger angles and longer wavelengths for larger dielectric thicknesses.

A common feature between all the trials shown in Figures 6-9 is that the resonance appears to broaden with increasing dielectric thickness, opening towards larger angles and longer wavelengths, respectively. The direction in which the resonances broaden can be seen by comparing the reflectivity of the samples with similar dielectric materials and different dielectric thicknesses to the left (smaller angles/shorter wavelengths) where the reflectivity curves are almost colinear, to the right (larger angles/longer wavelengths) where the curves diverge from one another as they approach their new baseline values.

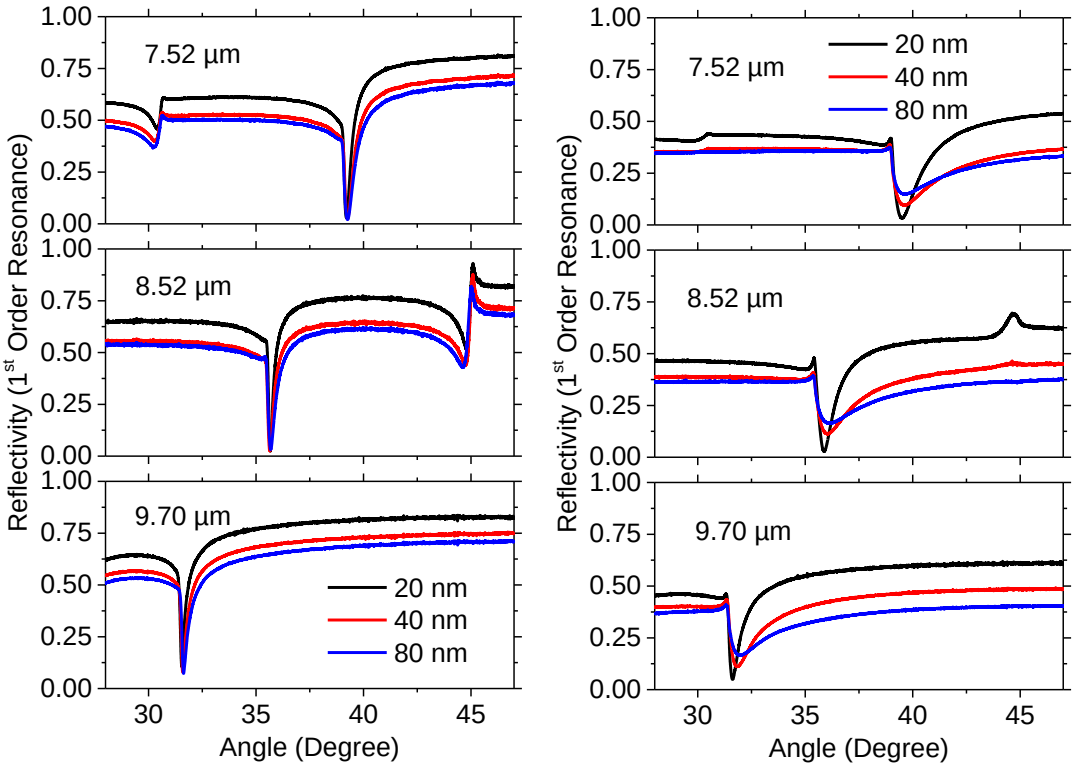

Figure 7(left), 8(right): Angular Sweep Dielectric Thickness Comparison, SiO_2 (Fig. 7) and TiO_2 (Fig. 8)

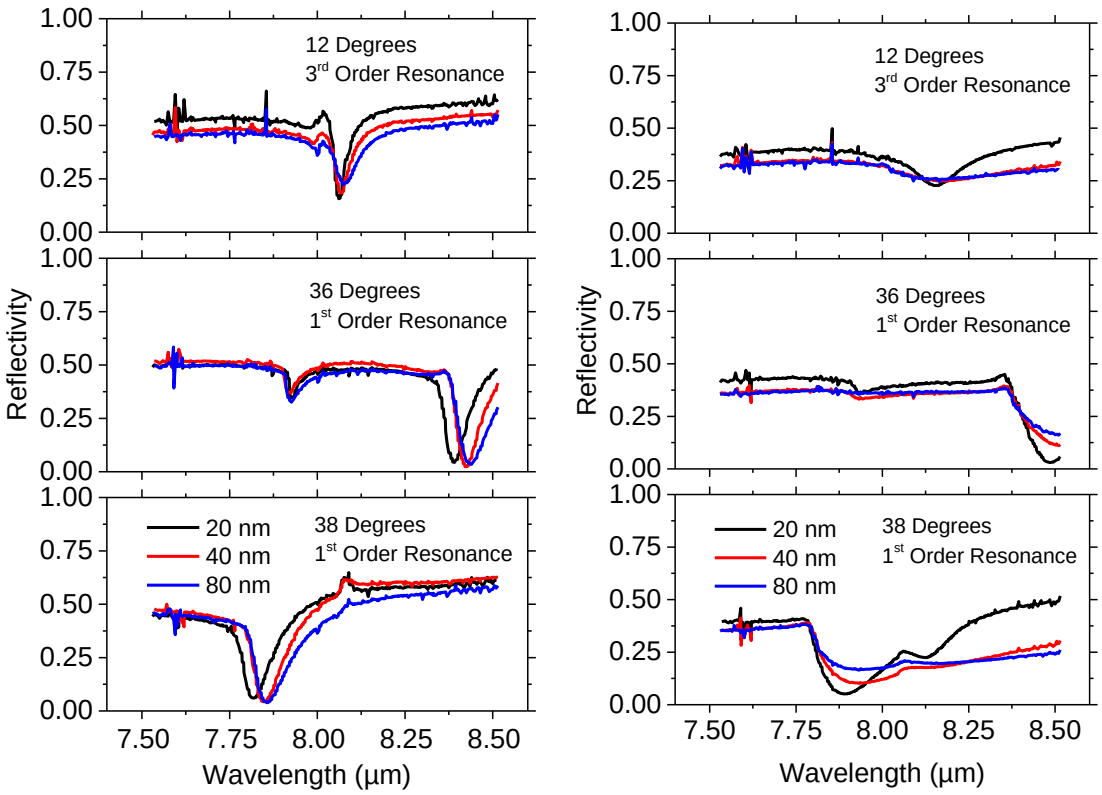

8

Figure 9(left), 10(right): Wavelength Sweep Dielectric Thickness Comparison, SiO_2 (Fig. 9) and TiO_2 (Fig. 10)

Figure 10 shows the reflectivity characterization of sample set 2 as a function of angle. This set contains devices with much thicker dielectric layers than those in sample set 1. The only material used in the fabrication of the layer in these devices was SiO_2. In every run for every device, there is some sort of reflectivity feature in a common location for every wavelength. Comparing to the results from the equivalent experiment performed in sample set 1, the general trend of the resonances broadening into the larger angles for thicker dielectric layers holds. It is apparent that there were no well-formed resonances achieved for devices with dielectric layers thicker than 80 nm.

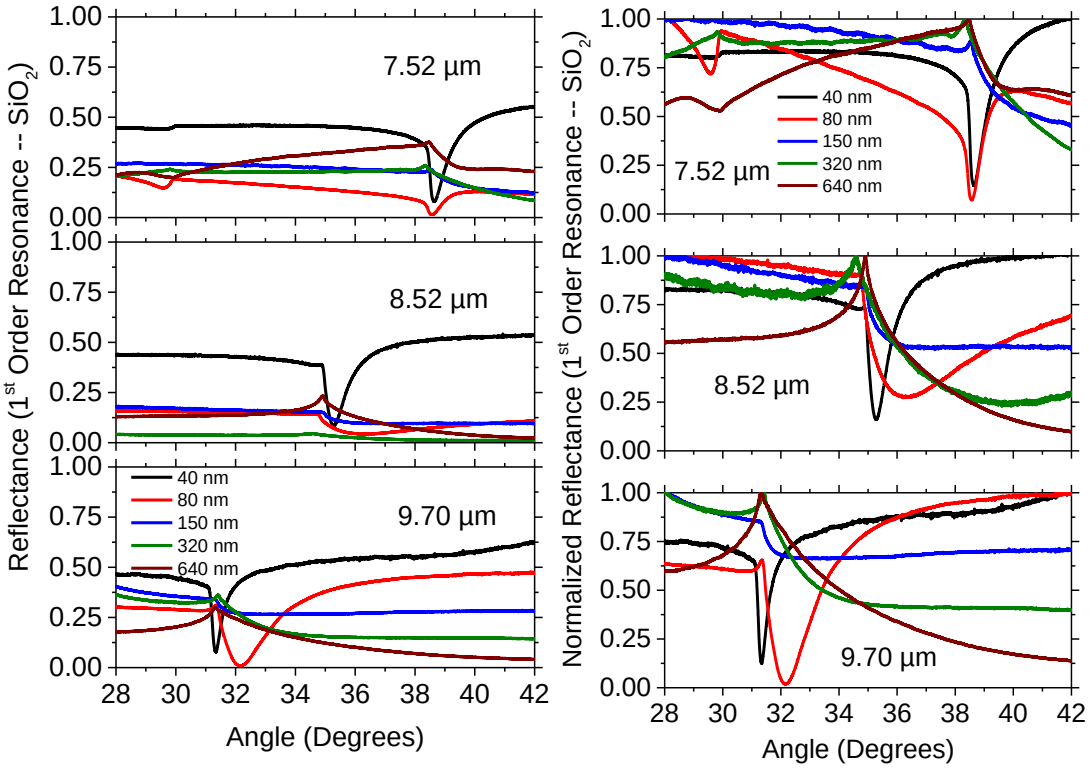

Figure 11(left), 12(right): Angular Sweep Dielectric Thickness Comparison of Sample Set 2 (Fig. 11 Raw Reflectivity, Fig. 12 Normalized)

Figure 11 shows the same data for the reflectivity of sample set 2, normalized over this angular range in order to account for the change in baseline reflectivity and better characterize the plasmonic features. This set contains devices with much thicker dielectric layers than those in sample set 1. The only material used in the fabrication of the dielectric layer in these devices was SiO_2. In every run for every device, there is some sort of reflectivity feature in a common location for every wavelength. Comparing to the results from the equivalent experiment performed in sample set 1, the general trend of the resonances broadening into the larger angles for thicker dielectric layers holds. It is apparent that there were no well-formed resonances achieved for devices with dielectric layers thicker than 80 nm, or about 1 % of the wavelength.

Most notably, we can see a well-formed resonance feature for the device with a 40 nm dielectric layer, as expected. However, the comparison between the 2 sample sets doesn't hold for the device with an 80 nm dielectric layer. In sample set 1 that device had a well-formed resonance feature at all 3 wavelengths, but in sample set 2 the corresponding device that had the same nominal parameters as in set 1 gave very different results. The devices with SiO_2 layers in sample set 1 had resonance features that showed no relation to wavelength for the angular sweep trials over the range that was utilized in this experiment. The devices in sample set 2 showed a larger variance of reflectivity for the different wavelengths, even though they were nominally the same as the ones in the other sample set and were manufactured with the same techniques. The only difference between these samples was the facility in which they were manufactured. While using different equipment can cause variations in the uniformity of the structures created, it is not anticipated that devices made with the same materials would show differences in their sensitivity to changing wavelength as was demonstrated between the two sample sets.

The final source of data that was characterized in support of this experiment was FDTD simulations (Fig. 12 and Fig. 13) that were analogous to the wavelength sweep characterization that was discussed earlier. In these simulations, dielectric thicknesses were varied from 0 nm to 200 nm, with a subset of the trials compiled to span the whole range of the dielectric layer thicknesses. The angles of incidence chosen as parameters for these simulations were 12^o, 36^o, and 38^o to match those angles shown used in the physical experiments detailed above.

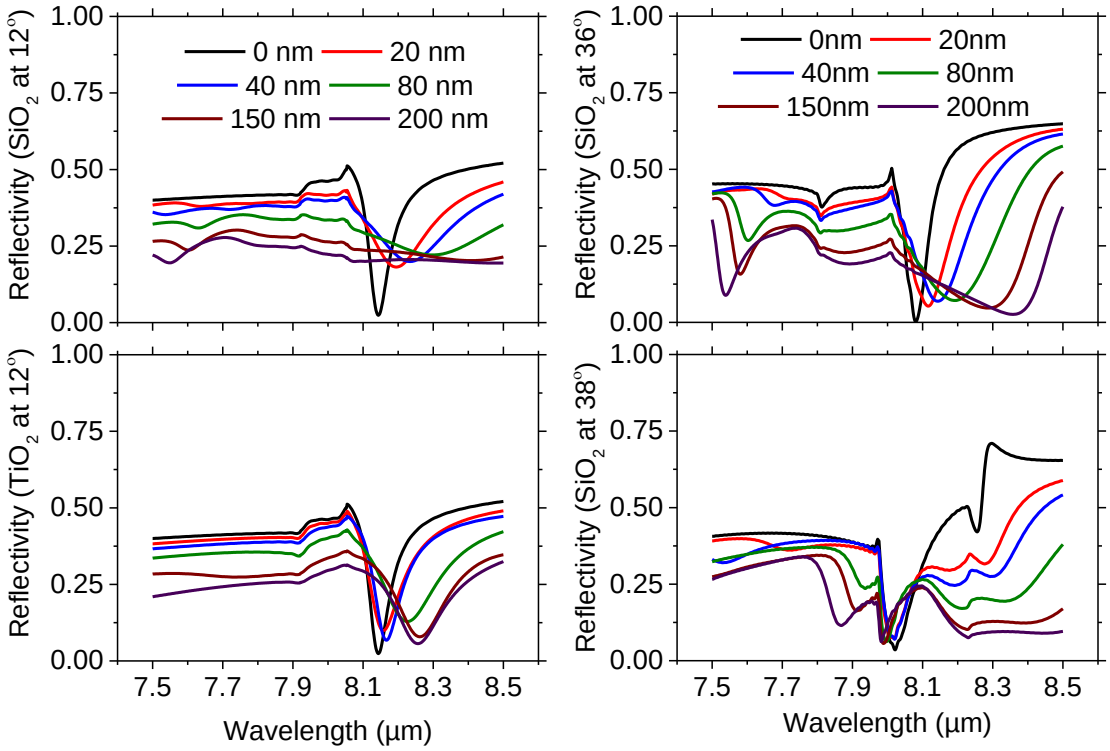

Figure 13(left), 14(right): Simulation Data of Wavelength Sweeps Thickness Comparison, 12° (F.13), 36° and 38° (F.14)

The general trends observed earlier that baseline reflectivity is decreased for devices with thicker dielectric layers, and that as the dielectric layer increases the resonance tends to broaden out into the longer wavelengths is supported by the simulation results. The simulations also show devices with SiO_2 as their layer dielectric as having markedly less pronounced resonance features for larger dielectric thicknesses than those with TiO_2 at an incidence angle of 12°. Finally, the resonance features simulated at an angle of 36° show a pronounced, linear shift of the resonance position into the longer wavelengths accompanying the resonance broadening for devices with thicker dielectric layers, however at 38° this broadening and shifting is less pronounced with the resonance positions staying constant with only a slight drift into the shorter wavelengths (the opposite direction than was observed experimentally).

CHAPTER FIVE: DISCUSSION

There are several discrepancies in the data presented above. These include a disagreement between sample sets 1 and 2 as to the wavelength dependence of resonance features for devices made with SiO_2 dielectric layers, a discrepancy between experiment and simulation regarding the direction of shifting resonance positions for SiO_2 dielectric devices at an incidence angle of 38^o, and another inconsistency between experiment and simulation regarding the resonance deformation properties of devices with SiO_2 vs. TiO_2 dielectric layers. To discuss these issues more qualitatively, the published optical constants for SiO_2 and TiO_2 have been plotted in figures 14, with some key values shown in Table 2[10]. Ellipsometry data for the dielectric films used in sample set 1 are provided as well (F.15). An important fact about these constants is that SiO_2 covers a much larger range of values for its refractive index (n) and extinction coefficient (k) than TiO_2, which is mostly constant in this wavelength range.

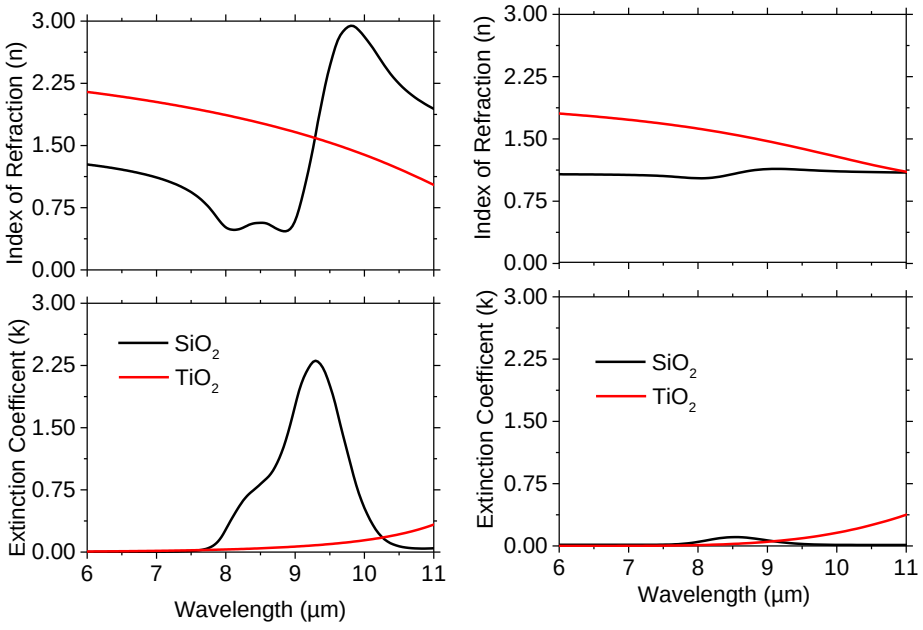

Figure 15(left), 16(right): Published Optical Constants for SiO_2 and TiO_2 (F.15)[10], and Measured Optical Constants for Dielectric Films Used in Sample Set 1 (F.16)

Table 3
Published Optical Constants for SiO_2 and TiO_2 at Important Wavelengths [10]

Important Optical Constants						
		SiO_2			TiO_2	
	7.52 μm	8.52 μm	9.70 μm	7.52 μm	8.52 μm	9.70 μm
n	0.92	0.57	2.87	1.95	1.76	1.48
k	0.02	0.84	1.35	0.02	0.04	0.11

As was mentioned before, the devices in samples sets 1 and 2 were nominally the same, with the only difference between them being the facilities in which they were manufactured. Following the argument presented in the results section, any geometric differences between the devices would not cause the change in wavelength sensitivity that was observed. This leads to the conclusion that the optical properties of the films in sample set 1 are different than those in sample set 2. Referring to table 1, the published values of SiO_2 show a variation in the n value of approximately 500% from 8.52 μm to 9.70 μm, with 7.52 μm having a value for n 200% that of 8.52 μm. The value of k for SiO_2 increases approximately linearly as wavelength increases over this range. Examining the reflectivity data for sample set 2 (Fig. 10), the resonance features stay together the best for the 9.70 μm trial and deteriorate the most in the 8.52 μm trial (7.52 μm trial is between them in quality).

Comparing these results to the published values of n and k discussed above, it is the authors hypothesis that the quality of the resonance features for these dielectric -grating devices is dependent on the refractive index (n) and not on the extinction coefficient (k). Higher values of n lead to stronger resonance features (see the above argument) while the value of k does not seem to have an effect. This is supported by the fact that, for SiO_2, at 8.52 μm the value of k is much larger than at 7.52 μm while the value at 9.70 μm is the largest of all three (if k was the parameter that determined resonance quality then we would expect quality to change strictly in one direction as wavelength increases, however this is not the case).

The index of refraction for the SiO_2 and TiO_2 films in sample set 1 appear to be constant over the range of inspected wavelengths, with the prediction that the TiO_2 index be smaller than that of the SiO_2. Comparing the results of the simulations to the data collected in the experiments, there is a much larger difference in terms of reflectivity vs. dielectric thickness for the simulations than for what was recorded. This stands to show that the optical constants used in the simulations were not in agreement with the constants of the films in sample set 1.

In conclusion, it was shown that surface plasma waves can be excited on dielectric - grating devices, provided the appropriate parameters are satisfied. Both the collected data and the simulation results support the hypothesis that resonance quality decreases with respect to increasing dielectric thickness. Finally, a theory was presented to explain the dependence of the dielectric material on resonance quality in which the refractive index (n) is the only optical parameter that influences the resonance, with the extinction coefficient (k) being of less importance. Future studies may wish to explore the optimization of dielectric layer material with the refractive index (n) as the parameter, and to vary the ground plane conductivity and characterize resonance quality.

LIST OF REFERENCES

[1] W. Barnes, A. Dereux, and T. Eddesen, "Surface Plasmon Subwavelength Optics," Nature 424, 824-830 (2003)

[2] I. R. Hooper and J. R. Sambles, "Surface Plasmon Polaritons on Thin-Slab Metal Gratings," Physical Review B 67, 235404 (2003)

[3] L. Landau and E. Lifshitz, "Electrodynamics of continuous media, vol. 8", *Pergamon Press,* (1960)

[4] J. Cleary, et al., "Long-Wave Infrared Surface Plasmon Grating Coupler," Applied Optics Vol. 49, No. 16, 3102-3110 (2010)

[5] R.S. Anwar, et al., "Recent Advancements in Surface Plasmon Polaritons-Plasmonics in Subwavelength Structures in Microwave and Terahertz Regimes," Digital Communications and Networks (2017)

[6] K. Gorgulu, et al., "All-Silicon Ultra-Broadband Infrared Light Absorbers," Nature Scientific Reports 6:38589 (2016)

[7] H. Kim, et al., "Tunable Directional Beaming from Subwavelength Metal Slits with Metal-Dielectric Composite Surface Gratings," Optics Letters Vol. 34, Vol. 17, 2569-2571 (2009)

[8] G. Zhen, et al., "Modes Coupling Analysis of SPP's Based Resonance Manipulation in Infrared Metamaterial Absorber," Nature Scientific Reports 7:46093 (2016)

[9] D. Cardimona and D. Huang, "New Optical Detector Concepts for Space Applications," *Proceedings in SPIE*, DOI: 10.1117/12.851072 (2010)

[10] J. Kischkat, et al. "Mid-infrared optical properties of thin films of aluminum oxide, titanium dioxide, silicon dioxide, aluminum nitride, and silicon nitride", *Appl. Opt.* **51**, 6789-6798 (2012) (Numerical data kindly provided by Jan Kischkat)